FEATURE ARTICLE

Aspects of Photoinduced Molecular Three-Body Decay

Christof Maul and Karl-Heinz Gericke*

Institut für Physikalische und Theoretische Chemie, Technische Universität Braunschweig,
Hans-Sommer-Strasse 10, D-38106 Braunschweig, Germany

New experimental techniques and novel analysis procedures promote the investigation of three-body processes. Photoinduced three-body decay can be studied by technologically advanced, challenging coincidence experiments as well as by established spectroscopic techniques if physically meaningful decay mechanisms and parameters are introduced. Such kinematic analysis procedures, based on the evaluation of fragment kinetic energy distributions, are presented, ranging from synchronous concerted via asynchronous concerted to purely sequential decay mechanisms. A Dalitz plot representation of a three-body decay is proffered, bridging the gap between established methods and novel coincidence techniques. Results for structurally similar molecules are presented: phosgene, carbonyl chloride fluoride, and thionyl chloride. Competing mechanisms govern the decay of phosgene via the X^1A_1 ground state and the A^1A_2 excited state potential energy surfaces. Carbonyl chloride fluoride behaves similarly, but the larger stability of the COF intermediate reduces the complexity brought about by decay channel competition and essentially confirms the phosgene results. Two electronic excited states determine the dynamics of the thionyl chloride decay leading to a competition between three- and two-body decay. Fragmentation from the second absorption band leads to results comparable to the phosgene decay via the A^1A_2 state.

I. Introduction

Studies of two-body photodissociation processes have vastly augmented our knowledge about chemical reaction dynamics. One logic development has been to investigate "full collisions" instead of "half collisions", i.e., going from photodissociation studies to investigations of bimolecular reactions. An equally logic development is to stay within the "half collision" domain, but to study more complex systems by increasing the number of fragments in the elementary process. This aims at the heart of many complex reaction schemes with three-body collisions as important steps, especially in atmospheric and combustion chemistry. The most prominent example for such a case is the ozone formation process $O_2 + O + M \rightarrow O_3 + M^*$, where the third collision partner M is needed to stabilize the newly formed ozone molecule.

In view of the fundamental significance of three-body processes in general, it is somewhat surprising that even for photoinduced three-body decay processes as their simplest example only relatively few studies exist leaving uncharted territory in the map of physical chemistry. The most general formulation of photoinduced three-body dissociation is given by

$$ABC + h\nu \rightarrow A + B + C \qquad (1)$$

where a molecule ABC breaks up into three fragments A, B, and C upon photon absorption. These fragments need not

necessarily be atomic, but can be radicals or molecules themselves, with internal structure and various degrees of freedom. For a complete description of the elementary process (1) it is therefore inevitable not only to determine the chemical nature and the kinematics of the fragments A, B, and C, but also their physical properties (angular momentum, internal energy) given by the quantum states q_A, q_B, and q_C. This additional complexity distinguishes reaction (1) from other three-body systems mainly studied in atomic physics, as e.g., double ionization of the helium atom,[1] total fragmentation of the hydrogen molecule H_2,[2] and also from the simplest example of molecular three-body decay: the three-body fragmentation of triatomic hydrogen H_3 into three neutral hydrogen atoms.[3] The additional complexity is also why we constrain ourselves to the discussion of photoinduced three-body fragmentation with well-defined initial conditions, and why we will not consider similar collision induced processes with usually ill-defined initial conditions.

To our knowledge, the first time when three-body decay was discussed as an elementary event in chemistry was 65 years ago when Norrish et al. found that "the primary decomposition of acetone occurs by way of free radicals: $CO(CH_3)_2 = CO + 2 CH_3$".[4] The authors also speculate on the dynamics of this process, but are forced to admit that "it is impossible to state whether these radicals are detached simultaneously, or the one rapidly followed by another".[4] The first investigation of three-body decay dynamics was performed by Kroger and Riley for the photodissociation of acetyl iodide, CH_3COI.[5] They found that acetyl iodide "photodecomposes to yield three fragments: I atoms, CO molecules and CH_3 radicals",[5] which beautifully

* To whom correspondence should be addressed. Phone: +49 (531) 3915326. Fax: +49 (531) 3915396. E-mail: k.gericke@tu-bs.de.

illustrates the remarks made above about fragment complexity in (1). By monitoring fragment velocity and angular distributions they found that the "photodissociation process can be modeled in two stages: initial impulsive recoil followed by statistical unimolecular decay" [5] of a long-lived acetyl fragment, where long life in this context means the survival of several rotational periods.

Since that time quite a few studies have been performed on numerous molecules by a variety of techniques. More often than not three-body decay has only been considered in order to explain unwanted effects obscuring desired information. Mostly, the main issue has been whether the two bonds A−B and B−C break in a concerted manner (or even simultaneously), or if the process is sequential in nature involving a long-lived intermediate AB particle. Only lately, systematic studies have focussed on the dynamics of three-body decays as such beyond the issue of concertedness or sequentiality, and recently the topic has extensively been reviewed for the first time.[6]

Experimental techniques include photofragment translational spectroscopy (PTS), resonance enhanced multiphoton time-of-flight measurements (REMPI/TOF), photofragment imaging (PI), ultrafast femtosecond spectroscopy, and coincidence measurements. The nonresonant electron impact ionization scheme of most PTS experiments guarantees a complete detection of all fragment species, but does not allow to obtain information on the internal fragment state population. This is the domain of spectroscopic techniques, such as REMPI/TOF, laser induced fluorescence (LIF), or photofragment imaging, which in turn cannot be employed to monitor spectroscopically dark fragments. These techniques rely on analyzing fragment kinetic energy distributions (KED) by kinematic or statistical reasoning in order to draw conclusions on the dynamics of the three-body decay process. Femtosecond experiments are unique in that they allow to directly determine fragment build-up times on the time scale of the vibrational motion of the parent molecule constituents. Coincidence techniques rely on the simultaneous detection of at least two coincidently generated photofragments from the same elementary process and thus eliminate the necessity to employ kinematic or statistic models in analyzing experimental data. Due to the demanding nature of coincidence experiments, up to date they have only been performed for the disintegration of previously positively or negatively charged parent molecules which had been accelerated to sufficiently high kinetic energies for the photofragments to be detected by the particle detector without further experimental effort.

The analysis of experimental data is far more complex than for the case of the corresponding two-body decay, and different approaches have been followed in order to gain insight into three-body decay dynamics. One such procedure, namely the kinematic analysis developed by the authors and based on physically meaningful decay models, will be outlined in some detail in the following chapter. Previously employed techniques, e.g., maximum entropy analysis, rely on statistical methods and are especially suited for analyzing data for larger polyatomic molecules.[7,8]

Numerous molecules have been investigated.[6] Their range includes acetone and related carbonyl compounds which have evolved as three-body decay working horses for their easily accessible breakup into three fragments at convenient dissociation wavelengths and short (partially halogenated) alkane chains, but also simple, fundamental molecules such as O_3,[9] Cl_2O,[10] ClO_2,[11] and H_2O.[12] Femtosecond experiments have mainly focused on the multiple bond breaking in acetone[13−15] and

several metal carbonyl compounds such as $Fe(CO)_5$ and $Cr(CO)_6$.[16,17] In coincidence studies, apart from studies on the three-body decay of charged particles like $Ar_n^+ + h\nu \rightarrow Ar_{n-2}^+ + 2\ Ar$[18,19] or $XYZ^{++} + h\nu \rightarrow X + Y^+ + Z^+$,[20] also neutrals like H_3 and O_6 have been investigated following charge transfer $(H_3^+ + Cs \rightarrow H_3 + Cs^+)$[3] or dissociative photodetachment $(O_6^- + h\nu \rightarrow O_6 + e^-)$[21] processes.

This article is intended to highlight specifics encountered in the investigation of three-body decay dynamics, to present some useful tools and to demonstrate their application to a series of structurally similar molecules. A more comprehensive review covering most of the above mentioned systems, which is beyond the scope of this work, can be found in ref 6.

II. Methods

In order to comprehend the specific problems and the proposed solutions encountered in the study of three-body dissociation processes, it is helpful first to recapitulate the general approach for investigating similar two-body fragmentation processes:

$$XY + h\nu \rightarrow X + Y \qquad (2)$$

Here, a complete kinematic analysis can be performed in a straightforward manner by observation of a single fragment, provided the observation is performed in a state and kinetic energy sensitive manner, e.g., by resonance enhanced multiphoton ionization combined with time-of-flight measurements (REMPI-TOF) or by sub-Doppler laser induced fluorescence detection (LIF). The evaluation of the energy balance in the center of mass frame of the parent molecule XY yields

$$E_{av} = h\nu - D_0(X-Y) + E_{XY} = E_X + T_X + E_Y + T_Y \quad (3)$$

where E_X, E_Y, and E_{XY} represent the internal and T_X and T_Y the kinetic energies of the respective particles X, Y, and XY. The available energy E_{av} is given by the difference of the well-defined photon energy $h\nu$ with the dissociation energy D_0 and the internal energy E_{XY} of the parent. If experiments are performed in a supersonic jet expansion, the internal energy E_{XY} of the parent molecule prior to the decomposition can be neglected due to its smallness. If, however, the fragmentation of state selected molecules is studied, e.g., by infrared overtone preparation, then E_{XY} is also well-defined. Observing one fragment, say X, by a state-selective, kinetic energy sensitive method yields E_X and T_X of the respective dissociation product X, leaving E_Y and T_Y of the partner product Y as unknown quantities, which are unambiguously determined by the conservation laws for linear momentum and energy.

The corresponding analysis of a three-body decay (1) is significantly more complex due to its underdetermined kinetic equations. Now, one has to deal with two additional terms, E_C and T_C, on the right hand side of the energy balance equation:

$$E_{av} = E_A + T_A + E_B + T_B + E_C + T_C \qquad (4)$$

Performing the same experiment as for the two-body case again yields two energy values, e.g., E_A and T_A. However, four instead of two unknown quantities remain on the right hand side of eq 4, only two of which are determined by the conservation laws.

The best solution to the outlined problem is to obtain additional experimental information by coincident observation of at least two fragments generated in the same elementary process. As a consequence of new technical developments,[22,23]

Feature Article

J. Phys. Chem. A, Vol. 104, No. 12, 2000 **2533**

this challenging approach is successfully being followed by several research groups on a variety of systems.[3,19,21,24] However, this technique has not yet been combined with state selective fragment observation, an experiment which is currently set up in our laboratory.

In order to achieve state and energy selectivity in a coincidence experiment, it is necessary to equip position sensitive particle detectors with a tunable light source which is powerful enough to ionize at least two of the neutral fragments, which have coincidently been generated in the three-body fragmentation, by a spectroscopic detection technique like REMPI. Other than in conventional coincidence experiments, the high power required for the nonlinear REMPI ionization process prohibits the use of a continuously emitting light source, but requires high power pulsed lasers.

Suitable particle detectors are, for example, multichannel plates (MCP) combined with delay-line anodes which determine the point of impact of the secondary electrons. Here, two sets of parallel wires form two wire planes orthogonal to each other which are coupled to a delay line.[25] The impact position is determined by measuring the time of arrival of the signal at each end of the delay line. The delay line signal arrival times are fed into a set of four time-to-digital (TDC) converters, two for each coordinate. If a multiplexing device is used, more than one particle can be monitored by a corresponding number of TDC sets. The respective impact positions define the initial x and y fragment velocity components perpendicular to the spectrometer axis by dividing the measured x and y position coordinates by the total TOF. The total TOF, hence the z component of the velocity along the spectrometer axis is obtained by coupling the MCP charging circuit to a fifth TDC per particle utilizing the same multiplexing scheme as for the other coordinates in order to assure multiparticle monitoring. Thus, the validity of coincidence events can be checked by the correct number of five stop counts per particle and by the correct complementary arrival times of the two signals at the opposite ends of each delay line. From the three-dimensional velocities of a coincident correlated fragment pair which are determined in this way, the three-dimensional velocity and the internal energy of the third partner fragment are unambiguously determined if the internal energies of the fragment pair are known.

To this end a laser is utilized for spectroscopic fragment detection by REMPI. If for simplicity the experiment is designed as a one-color experiment, the laser has to supply four photons per fragment, if a (2+1) REMPI detection scheme is utilized— one for dissociation, two for resonant excitation, one for ionization, where the two-photon resonant excitation is the step with the least excitation cross section. Of the total two-event count rate, only some fraction will be real coincidence events, i.e., caused by fragments generated in the same elementary process, while the remaining counts are false coincidences caused by two fragments from two different elementary processes. The ratio of false to real coincidence events is $2(n-1)$, where n is the number of molecules in the observation region. Only for the case $n = 1$ the number of real coincidence events exceeds the number of false coincidence events. Therefore the sample must be sufficiently diluted to ensure that only one parent molecule is in the observation region defined by the laser focus volume.

If saturation of the two-photon resonant excitation is achieved and the parent molecule density is maintained at one particle per laser focus volume, then one coincidence event is generated per laser pulse, yielding a coincidence count rate of ca. 10 cps

at a laser repetition rate of 100 Hz and a spectrometer detection efficiency of 30%. Two-photon excitation saturation can be achieved by modern commercial dye laser systems: 1.5 mJ/ pulse at (one-photon) excitation wavelengths between 220 and 250 nm at a pulse duration δt of 3 ns result in a photon flux I of ca. 5×10^{29} photons/cm²s for a focus cross section of 10^{-6} cm². Typical two-photon cross sections σ are 10^{-45} to 10^{-50} cm⁴ s, fulfilling the saturation condition $\sigma I^2 \delta t \geq 1$. Thus, three-body dissociation processes generating two atomic hydrogen, oxygen, or chlorine fragments can be completely characterized by the new experimental setup.

If coincident fragment observation is not feasible, the solution for dealing with the underdetermined kinematic three-body decay equations is to introduce additional constraints for the interrelationship of the six internal and kinetic fragment energies E_A, E_B, E_C, T_A, T_B, and T_C. Thus, the necessity of performing coincidence experiments is replaced by a suitable parametrization of the decay process involving few parameters which reflect the joint probability distribution $P(E_i, T_i)$ ($i = A, B, C$) to a high degree of accuracy if P is smooth and does not exhibit more than two maxima. The latter condition is likely to be fulfilled if the photon energy is not very much higher than the three-body dissociation energy. To implement such a kinematic analysis procedure one must impose appropriate decay models relying on few physically meaningful decay parameters P_i. Here, the main issue to be addressed is whether the two bonds A−B and B−C break in one single kinetic event at time τ or in two independent steps at times τ_1 and τ_2, i.e., if upon a closer look reaction 1 becomes

$$\text{ABC} + h\nu \rightarrow \text{ABC*} \xrightarrow{\tau} \text{A} + \text{B} + \text{C} \qquad (5a)$$

or

$$\text{ABC} + h\nu \rightarrow \text{ABC*} \xrightarrow{\tau_1} \text{AB*} + \text{C} \xrightarrow{\tau_2} \text{A} + \text{B} + \text{C} \qquad (5b)$$
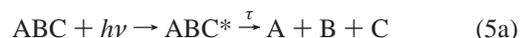
Here, the asterisk denotes molecules excited above their dissociation limit. Reaction 5a represents a synchronous concerted three-body decay, while (5b) stands for a purely sequential three-body decay, if the time span $\Delta t = \tau_2 - \tau_1$ is greater than the mean rotational period τ_{rot} of the intermediate fragment AB, and for an asynchronous concerted three-body decay, if $0 < \Delta t \leq \tau_{rot}$.[8] The latter distinction is necessary, because for $0 < \Delta t \leq \tau_{rot}$ the decaying AB intermediate will possess a memory of the geometry and the orientation of the parent molecule ABC at the time τ_1 of the first bond cleavage B−C, while for $\Delta t > \tau_{rot}$ such a memory will be lost except for the conservation of total angular momentum.

A very illustrative, yet oversimplifying picture of synchronous and asynchronous concerted fragmentation of a linear symmetric ABA molecule involves the excitation of symmetric or antisymmetric stretching modes in the parent. Symmetric vibration lengthens both bonds A−B in phase, causing both fragments A to be ejected from the parent at exactly the same time: $\Delta t = 0$, which is characteristic for a synchronous decay. Antisymmetric vibration with a period τ_{vib} leads to the lengthening of one A−B bond along with the contraction of the other A−B bond. Hence, bond length oscillations are phase-shifted by π, and the departure of the second A fragment will take place half a vibrational period later than the ejection of the first one: $\Delta t = \tau_{vib}/2$, which is characteristic for an asynchronous decay. The energy transfer onto the fragments will be different because of the different respective "collision partners".

The motivation for the parametrization procedure is to establish relationships between parameter value distributions
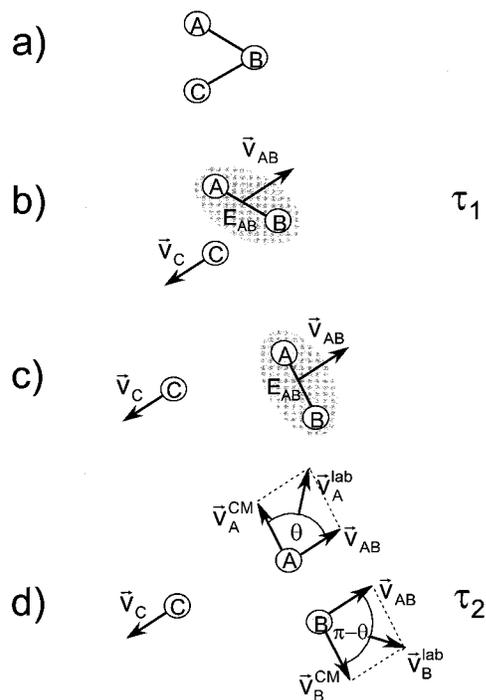
Figure 1. Illustration of a sequential decay mechanism. (a) The ABC parent of arbitrary geometry decays at time τ_1 (b) into the final fragment C and into the intermediate fragment AB. The speeds of the final fragment C and the intermediate AB depends on the energy deposition E_{AB} in the intermediate. (c) After further separation of the AB–C system, at time τ_2 (d) the AB intermediate decays into the final fragments A and B. The laboratory speeds of the final fragments A and B do not only depend on E_{AB}, but also on the decay angle θ.

$f_i(P_i)$ and fragment kinetic energy distributions $f_j(T_j)$ (KEDs) which are characteristic for the above discussed decay mechanisms: $f_j(T_j) = F_j(f_i(P_i))$. Here, i numbers the parameters and j the fragments, respectively. Having performed measurements on the KEDs of one or, better, more fragments from a three-body dissociation (without coincident observation), the inverted relationships F_j^{-1}) can be used to draw conclusions on the decay mechanism and the parameter distributions from the observed data. For a detailed general discussion the reader is referred to our recent work.[6,26] In the following, selected illustrative examples for these relationships will be presented.

The simplest case to be modeled is the synchronous concerted mechanism. Here, it is obvious that the momentum transfer onto the final fragments A and C must be equal, and that the kinetic energy content in all fragments exclusively depends on the bond angle at time τ. Large bond angles correlate with large kinetic energies of the terminal A and C fragments, small bond angles correlate with small kinetic energies for A and C. For the central B fragment the correlation is simply reversed. Due to its simplicity, this parametrization has been used in three-body decay analysis before. However, neglecting nonsynchronous pathways has not always yielded perfectly matching results.[27,28]

The nonsynchronous decays can be modeled as illustrated in Figure 1. The ABC parent of arbitrary geometry (cf. Figure la) decays at time τ_1 into the final fragment C and into the intermediate fragment AB (cf. Figure 1b). The velocities, and hence the kinetic energies, of AB and C are determined by the known available energy E_{av}, the observable internal energy E_C of fragment C, and the nonobservable energy deposition parameter E_{AB} in the intermediate. Here, E_{AB} accounts for excitation beyond the dissociation limit of AB[29] and can be electronic, vibrational, or rotational in nature. After further separation of the AB–C system (cf. Figure 1c), at time τ_2 the

AB intermediate decays into the final fragments A and B (cf. Figure 1d). Now, the kinetic energy release in the center of mass system of AB is governed by the energy deposition E_{AB} (diminished by the observable internal fragment energies E_A and E_B, where applicable). However, the kinetic energies T_A and T_B are measured in the laboratory system. Therefore, the velocity v_{AB} of the intermediate, acquired in the first B–C bond cleavage, and the AB center of mass velocities v_A^{CM} and v_B^{CM} of the fragments must be added up to obtain the observable fragment laboratory velocities v_A^{lab} and v_B^{lab}. Thus, the laboratory velocities not only depend on the energy deposition E_{AB}, but also on the decay angle θ of v_{AB} with v_A^{CM} (or the angle $\pi-\theta$ of v_{AB} with v_B^{CM}). If no internal energies are present, the following relationships hold:

$$\frac{m_{AB}}{\mu}T_A = \frac{\mu}{m_B}E_{av} + \left(\frac{m_B}{\mu} - \frac{\mu}{m_B}\right)E_{AB} + 2\cos\theta\sqrt{E_{av}E_{AB} - E_{AB}^2} \tag{6a}$$

$$\frac{m_{AB}}{\mu}T_B = \frac{\mu}{m_A}E_{av} + \left(\frac{m_A}{\mu} - \frac{\mu}{m_A}\right)E_{AB} + 2\cos\theta\sqrt{E_{av}E_{AB} - E_{AB}^2} \tag{6b}$$

$$T_C = \frac{m_{AB}}{m_{ABC}}(E_{av} - E_{AB}) \tag{6c}$$

Here, m_{ABC} is the ABC parent molecule mass, and μ is the reduced mass of the ABC system: $\mu = \sqrt{m_A m_B m_C / m_{ABC}}$. The general case, where internal fragment excitation is considered, is discussed in refs 6 and 26. Once the relationships (eq 6) are established, it is straightforward to calculate fragment KEDs from arbitrary parameter distributions. For an illustration Figure 2 shows a series of simulated fragment KEDs for various conditions. In Figure 2a four KEDs are displayed for fragment B. The top trace illustrates a planar, purely sequential case ($f_\theta(\theta)$ = const), where also no preferred value for E_{AB} exists ($f_{AB}(E_{AB})$ = const). The corresponding KED is broad and unstructured, with no specific value for the kinetic energy content of B being favored above others. The lower three traces of Figure 2a were calculated for a relatively broad Gaussian distribution of the energy deposition E_{AB} around the center $E_{AB,0}$ of the distribution at $^1/_2E_{av}$. From top to bottom, they represent KEDs corresponding to a sequential decay ($f_\theta(\theta)$ = const) and a broad and a narrow decay angle distribution for asynchronous concerted back scattering of fragment B, where back scattering means a decay angle distribution centered around the value θ_0 = π. The sequential decay exhibits a bimodal, symmetrically shaped KED with the fast and the slow peaks corresponding to forward and backward scattering of fragment B. For the asynchronous concerted back scattering cases, the slow peak dominates while the fast peak vanishes the more, the narrower the decay angle distribution becomes. Similarly, any combination of parameter distributions $f_i(P_i)$ corresponds to certain fragment KEDs $f_j(T_j)$.

Figure 2b shows the KEDs for all fragments for asynchronous concerted back scattering of fragment B. The predominantly slow, backwards scattered B fragments correlate with predominantly fast, forward scattered A fragments, while the KED for fragment C simply reflects the distribution of the energy deposition E_{AB} in the intermediate.

The methods outlined above have been applied to a series of carbonyl and thionyl compounds. These play a major role for the investigation of three-body decay processes for two reasons. First, their dissociation energy with respect to fragmentation into three products is comparatively low, i.e., generally below

Feature Article

J. Phys. Chem. A, Vol. 104, No. 12, 2000 **2535**
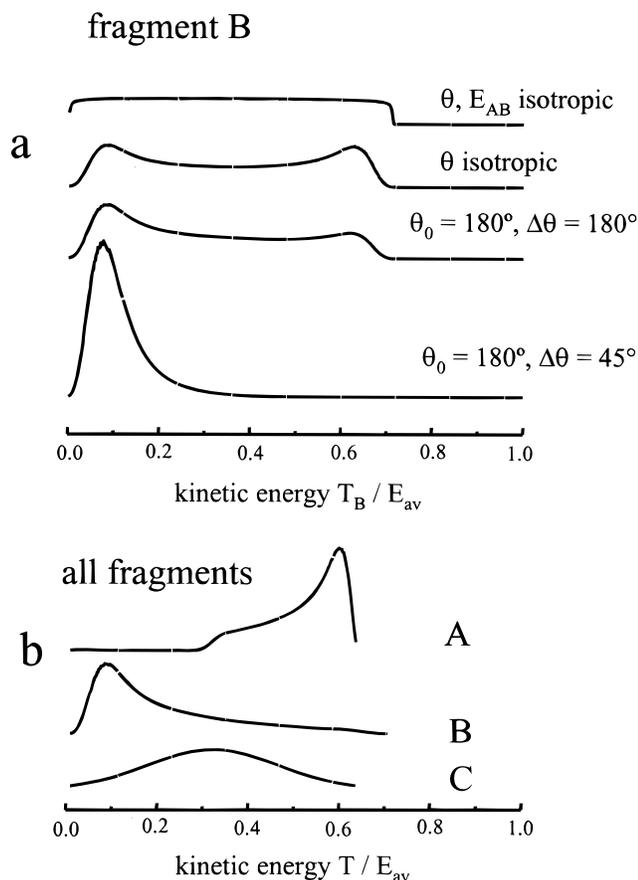
Figure 2. Simulation of kinetic energy distributions (KEDs) from given parameter distributions. (a) KEDs for fragment B. The top trace illustrates a planar, purely sequential case. The lower three traces of Figure 2a were calculated for a Gaussian distribution of the energy deposition around $E_{AB,0} = {}^1/_2E_{av}$. From top to bottom, they represent KEDs for a sequential decay, a broad and a narrow decay angle distribution for asynchronous concerted back scattering ($\theta_0 = \pi$). (b) KEDs for all fragments for asynchronous concerted back scattering of fragment B.

Figure 3. Energetics for the ultraviolet dissociation of $COCl_2$, COFCl, and $SOCl_2$. The two- and three-body energy domains are marked.

III. Experimental Section

A detailed description of the experimental setup has been given elsewhere.[30] Basically it consists of a crossed laser/molecular beam apparatus attached to a home-built single-field TOF spectrometer. The gaseous samples were fed into the spectrometer via a supersonic jet, generated in an inductively driven pulsed nozzle (General Valve Series 9/Iota One).

Simultaneous dissociation of the parent molecule and state-selective fragment detection was performed using a dye laser (Lambda Physik LPD 3000 or Lambda Physik ScanMate) pumped by an excimer laser (Lambda Physik LPX 605i or Lambda Physik LPX 100) or by a Nd:YAG laser (Coherent Infinity). The dye laser output was frequency doubled by a BBO crystal and focused into the spectrometer. It intersected the molecular beam at an angle of 54°, while the spectrometer formed an angle of 90° with the propagation direction of the laser beam. The angle between the spectrometer axis and the electric field vector of the linearly polarized laser light could be varied from 0° to 90° in order to investigate the spatial fragment distribution. The intensity of the laser light and the particle density in the supersonic beam were carefully controlled to avoid kinetic energy transfer onto the fragments due to space charge effects. The fragments were ionized by resonance-enhanced multi-photon ionization (REMPI). SO fragments[31] were detected in a (1+1) REMPI scheme, Cl fragments,[32] and CO fragments[33] in a (2+1) REMPI scheme in the wavelength range between 230 and 237 nm.

The experiment was operated in three modes: (a) the drift mode, (b) the acceleration mode, and (c) the Doppler mode. In all modes the ions are detected by a double stage multi-channel plate assembly (Galileo) with an active diameter of 40 mm. In the drift mode no acceleration field is applied. In this case the spectrometer simply consists of a drift tube with length $s = 58$ cm, and the time of flight t is inversely proportional to the (laboratory) speed v_{lab} of the ion $t = s/v_{lab}$. After passing a discriminator (FAST 7011), the ion signal is monitored by a multihit time-to-digital converter (FAST 7885) with an adjustable time resolution between 5 and 80 ns, and stored in a data buffer (FAST MCD/PC). Typical acquisition times for a single TOF profile are 3000 s with a total of 3×10^5 ion counts. This mode is highly accurate for determining kinetic energies, but insensitive to slow particles due to the laboratory to center of mass transformation that has to be performed when working in a supersonic expansion.

6 eV, giving rise to easily accessible absorption bands in a spectral regime with wavelengths greater than 200 nm. Second, SO and CO products can easily be detected by a state-selective and energy-sensitive method as, for example, REMPI/TOF. If the remaining constituents of the compound are chosen such that they are likewise detectable, for example, Cl, the most complete characterization of internal and kinetic fragment energies, which can be achieved by noncoincidence methods, becomes possible.

The essential results obtained from a series of experiments on structurally similar molecules will briefly be outlined. The investigated molecules include phosgene ($COCl_2$), carbonyl chloride fluoride (COFCl), and thionyl chloride ($SOCl_2$). The reason for this choice was, apart from the fact that three-body decay takes place and that the respective fragments are detectable, that the influence of chemical substitutions in a molecule on the decay characteristics can be studied in detail. This is especially the case for the two carbonyl compounds. All investigated molecules are of a starlike configuration with a central C or S atom. The ground state carbonyl compounds are planar and exhibit C_{2v} ($COCl_2$) and C_s (COFCl) symmetries, respectively, while ground state $SOCl_2$ is nonplanar and belongs to the C_s point group. All molecules were photodissociated in a one-color experiment in the 230−237 nm wavelength region. The corresponding energy diagrams and the two-body and three-body decay regions are shown in Figure 3.

In the acceleration mode ions are accelerated by a moderate static electric field of typically 10^3 V/m in the acceleration region and detected after passing the drift tube. Here, ions are mass selected, and instead of the total speed, the measured quantity is the velocity component v_z along the spectrometer axis, monitored by mass peak broadening. A linear relationship between the velocity component v_z and the deviation Δt from the center of the TOF profile holds for our spectrometer geometry. Since the velocity component v_z is perpendicular to the velocity of the molecular beam, no laboratory to center of mass transformation has to be performed in this case. The ion signal is monitored by a digital oscilloscope (LeCroy 9450). This procedure is sensitive for all velocities down to zero, but due to the shorter flight times, the accuracy in the determination of kinetic energies is lower than in the drift mode. Combining the two modes yields experimental data both with the high accuracy of the drift mode and the completeness of the acceleration mode.

The Doppler mode employs strong acceleration fields in the order of 10^4 V/m to exclude ion fly-out, i.e., particles missing the detector due to large off-axis velocity components. This mode serves for mass selection and the determination of quantum state populations. Although the Doppler broadening of the spectral lines has not been used for obtaining KEDs due to the much lower accuracy as compared to the evaluation of the TOF data, it is a valuable tool to check for the correctness of the KEDs, derived from the TOF measurements, by an independent method.

The kinetic energy resolution is energy dependent and is approximately 5% for the energy values encountered here. For all acquisition modes, immediately after each measurement the background signal was monitored with the laser delayed with respect to the gas pulse under otherwise identical conditions and subtracted from the previously obtained TOF profile. Further data processing was performed by a personal computer.

IV. Phosgene: $COCl_2$

In the near ultraviolet dissociation of phosgene two chlorine atoms and a carbon monoxide molecule are produced:[34]

$$COCl_2 + h\nu(235 \text{ nm}) \rightarrow CO + 2Cl \qquad (7)$$
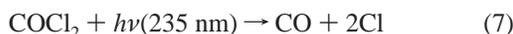
Both nascent CO and Cl REMPI Doppler and TOF spectra were obtained. A REMPI Doppler spectrum of nascent CO from phosgene photolysis at 230 nm shows significant rotational excitation up to $J = 65$ in $v = 0$ and $J = 55$ in $v = 1$, as is seen in the upper portion of Figure 4 for the 0-0 band of the $B^1\Sigma^+ \leftarrow X^1\Sigma^+$ transition. Two drift mode TOF profiles, obtained for selected quantum states, namely, for $J = 31$ and $J = 61$ which are marked in the upper spectrum, are shown in the lower part of Figure 4. Not surprisingly, the TOF increases with increasing internal (rotational energy), corresponding to lower kinetic fragment energies. A detailed analysis of acceleration and drift mode TOF spectra[6] yields KEDs like the one shown in Figure 5 for $v = 1$, $J = 34$. A least squares fit procedure involving only one of the decay mechanisms described above does not yield satisfactory matches to the experimental data. Only when competing decay mechanisms are allowed, a good agreement is obtained, as is also shown in Figure 5. Altogether 6 quantum states in $v = 0,1$ have been characterized in this manner, where the results are almost unspecific with regard to the investigated eigenstate.[35] All KEDs are broad, extending up to the energetic limit, and exhibit a bimodal shape.

Additionally, the chlorine partner fragments were characterized by the same techniques. Acceleration and drift mode TOF
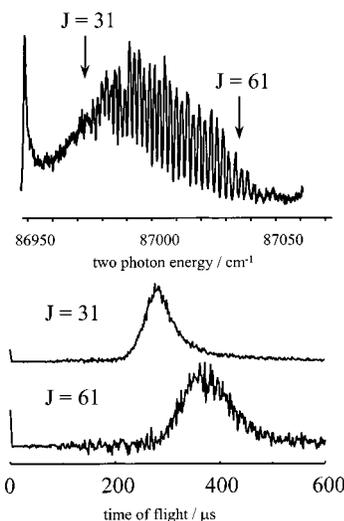
Figure 4. CO spectra (a) in the Doppler mode and (b) in the drift mode. The drift data were obtained for the selected resonance lines marked in (a).
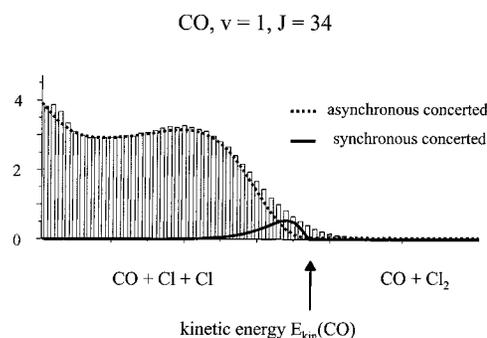
Figure 5. Kinetic energy distribution for a selected CO quantum state ($v = 1$, $J = 34$) derived from combined drift and acceleration mode measurements. The solid and the broken lines are best fits for the respective contributions of the asynchronous and the synchronous concerted mechanisms. Bar graph rather than continuous representation was chosen as a consequence of the kinetic energy binning in the analysis procedure. Numbers on the ordinate give the percentage of fragments in the respective kinetic energy interval.
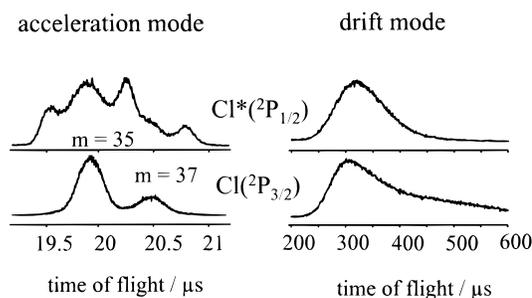
Figure 6. Figure 6. Drift and acceleration mode TOF spectra for excited spin−orbit state Cl*(^{2}P^1/$_2$) and ground state Cl(^{2}P^3/$_2$) atoms from the three-body decay of phosgene.

profiles are shown in Figure 6, and the corresponding KEDs for the two chlorine spin−orbit states which differ by only $E_\Omega = 881$ cm^{-1} in energy are depicted in Figure 7. Clearly, the two spin−orbit states exhibit a dramatically different behavior with respect to kinetic energy release. While both spin−orbit states are characterized by a bimodal KED, the slow component accounts for only 27% of the total excited state Cl*(^{2}P$_{1/2}$) yield, but for 83% of the total ground state Cl(^{2}P$_{3/2}$) yield.[36]

Considering the above mentioned experimental results, the following picture of the phosgene three-body decay is ob-

Feature Article

J. Phys. Chem. A, Vol. 104, No. 12, 2000 **2537**
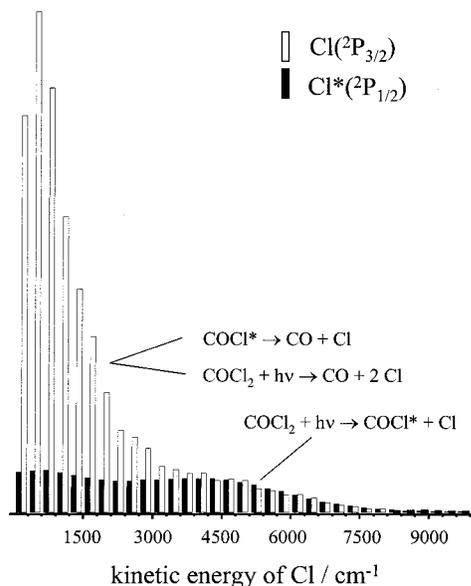
Figure 7. Kinetic energy distribution for atomic chlorine fragments from the three-body decay of phosgene derived from the data of Figure 6. Bar graph rather than continuous representation was chosen as a consequence of the kinetic energy binning in the analysis procedure.

tained: No significant contribution of a molecular channel, producing molecular chlorine molecules, is found. Likewise, the generation of a stable chloroformyl radical can be ruled out so that every dissociation process upon irradiation around 230 nm yields three fragments, two chlorine atoms and a carbon monoxide molecule. For this three-body decay, the asynchronous concerted mechanism is the dominant dissociation channel, accounting for more than 50% of the products. The chlorine fragments move preferentially in the same direction, resulting in forward scattering of the carbon monoxide. A less abundant decay channel is the synchronous mechanism, in which the two bonds cleave in unison and that accounts for the remaining products. The geometry of the decaying parent resembles the ground state equilibrium geometry with significant excitation of the $COCl_2$ bending modes. For both mechanisms the CO fragments are generated with high internal excitation. The competing fragmentation channels can be associated with the dissociation taking place after $\pi^*_{CO} \leftarrow n_{Cl}$ excitation in competition either directly on the excited $A(^1A_2)$ state or after internal conversion on the ground $X(^1A_1)$ state potential energy surface.[37]

The conclusions drawn from the Cl and the CO sets of observations agree nicely if the fact is taken into account that the chlorine data are contributed to by all CO partner fragments independently of the respective CO quantum state, while the CO data cannot include contributions from spectroscopically dark CO quantum states. Unfortunately, higher CO vibrational levels than $v = 1$ rapidly predissociate prior to ionization, so that a significant portion of highly excited CO fragments escapes direct detection. In order to decide whether our view of the phosgene dissociation process is realistic, a separate investigation of the first step of the asynchronous decay mechanism would be of great use.

In principle, an experiment that solely investigates the first step in the $COCl_2$ three-body decay could be realized by appropriately lowering the dissociation energy. However, the three-body threshold for $COCl_2$ is too low in energy (28700 cm^{-1}) for the molecule to absorb at the respective wavelengths. An alternative means is to chemically stabilize the intermediate
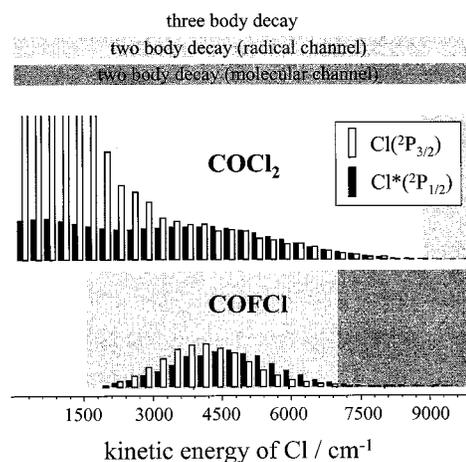
Figure 8. Kinetic energy distributions for atomic chlorine fragments from the three-body decay of phosgene and from the photodissociation of carbonyl chloride fluoride in direct comparison. The COFCl contribution resembles the distribution of the fast component in the phosgene KED. Bar graph rather than continuous representation was chosen as a consequence of the kinetic energy binning in the analysis procedure.

particle which in this case can easily be done by the fluorination of phosgene.

V. Carbonyl Chloride Fluoride: COFCl

The COF radical exhibits a well depth in the ground state potential energy curve of 9700 cm^{-1} compared to the COCl radical which is characterized by a well depth of only 5850 cm^{-1}.[38,39] According to Figure 3 the photon energy $h\nu$(235 nm) = 42550 cm^{-1} is only slightly above the three-body threshold at 40125 cm^{-1}, so that under the given experimental conditions exclusively products from the two-body decay can be monitored, because taking into account the collective translational motion of the molecular beam, the three-body decay fragments do not arrive at the detector within the monitored time interval of 600 μs. Thus, the conditions for observation of only the first step of the asynchronous concerted mechanism are fulfilled. Following the interpretation of the phosgene data one would expect the generation of fast chlorine atoms in both ground and excited spin−orbit states.

As shown in Figure 8, upon comparison of the chlorine atom KEDs from phosgene and carbonyl chloride fluoride fast chlorine atoms clearly dominate the dissociation process of COFCl. For COFCl the contributions of ground and excited spin−orbit state chlorine atoms are of equal magnitude, confirming the view of the dissociation process obtained from the more complex phosgene data that the first step in the asynchronous concerted decay channel produces fast chlorine atoms in both spin−orbit states while the second step as well as the synchronous concerted mechanism produce slow ground state atoms exclusively. While the available energies for the 235 nm dissociation of phosgene ($E_{av}[COCl_2] = 14800$ cm^{-1}) and of COFCl ($E_{av}[COFCl] = 12450$ cm^{-1}) are of equal magnitude, the mean internal excitation of the COF intermediate $\bar{E}$ (COF) = 4350 cm^{-1} is higher by about a factor of 2.5 than the corresponding mean excitation in the (unstable) COCl intermediate $\bar{E}$(COCl) = 1650 cm^{-1}, which simply reflects the larger stability of the COF radical.

Thus, the chemical substitution by fluorination of phosgene fully supports the view which was obtained by the kinematic analysis of the complex dissociation process of phosgene which,
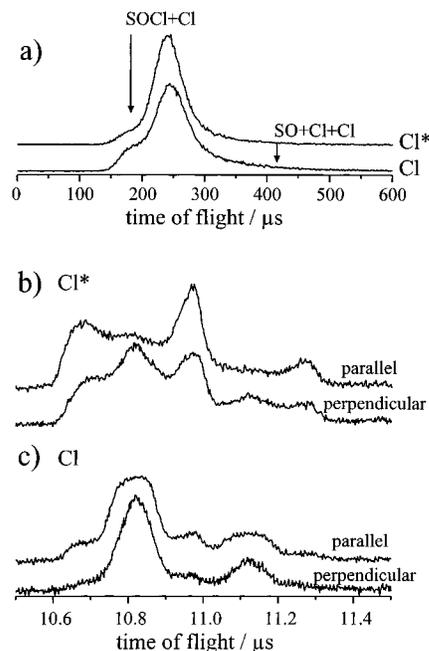
Figure 9. Drift (a) and acceleration mode (b, c) TOF spectra for excited spin-orbit state Cl*($^2P_{1/2}$) and ground state Cl($^2P_{3/2}$) atoms from three- and two-body decay of thionyl chloride. Additionally, acceleration mode profiles are shown for parallel and perpendicular polarization geometries.

contrary to the COFCl case, is governed by a competition of different three-body decay channels.

VI. Thionyl Chloride: SOCl$_2$

The chemical substitution replacing the central carbon atom in phosgene for a sulfur atom should yield results more different from the phosgene data than in the case of COFCl. This is easily rationalized if the different electronic properties of the respective central atoms are considered. In the molecular orbital picture the phosgene as well as the COFCl excitation is accomplished by a (forbidden) $\pi^* \leftarrow n$ transition in the CO double bond. For SOCl$_2$ the excitation wavelength $\lambda = 235$ nm lies, contrary to the cases for phosgene and COFCl, halfway between the first and the second absorption maxima.[40] Therefore, competing pathways are also expected, but based on the simultaneous excitation of different excited states rather than based on a competition between different exit channels from a single prepared excited parent molecule state. A qualitatively different behavior for the decay from the two possibly excited states of thionyl chloride has previously been observed in a series of experiments on the photodissociation at wavelengths of 193 and 248 nm, respectively. From long to short wavelengths, the decay character markedly changes from two-body to three-body.[41−45]

Previously, only ground state Cl($^2P_{3/2}$) atoms have been detected as primary photoproducts from SOCl$_2$ photodissociation between 224 and 254 nm.[40] With the present experimental REMPI-TOF setup also the nascent production of excited spin−orbit state Cl*($^2P_{1/2}$) was observed. From the drift and acceleration mode TOF profiles shown in Figure 9 for both Cl and for Cl* fragments, it is clear that the dissociation mechanism is indeed more complex than for the carbonyl compounds. Altogether three contributions can be identified: (I) three-body decay into SO + 2 Cl, (II) two-body decay into SOCl + Cl, and (III), to a minor extent, secondary photolysis of SOCl formed in process (II).[46] Due to the complementary detection
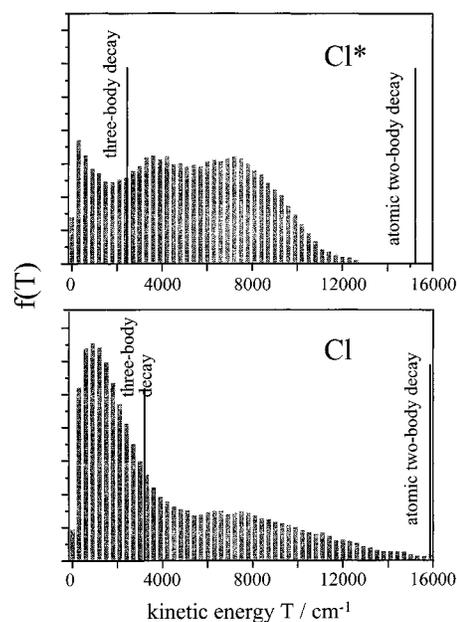
Figure 10. Kinetic energy distributions for atomic chlorine fragments from three- and two-body decay of thionyl chloride. Bar graph rather than continuous representation was chosen as a consequence of the kinetic energy binning in the analysis procedure.

efficencies of the two operation modes the acceleration mode profiles are contributed to by processes (I) and (II) only, while the drift mode profiles contain essentially information about channels (II) and (III). All processes exhibit spatially anisotropic fragment distributions, which is most pronounced for channel (II) and is evidence for fast atomic rearrangement on the picosecond or sub-picosecond time scale.

Due to the large three-body threshold of 37950 cm^{-1}, the total kinetic energy release into all fragment molecules must be small (less than 4550 cm^{-1}). As a consequence of this small energy release, electronically excites states of SO cannot be accessed. The corresponding maximum kinetic energy releases into the atomic chlorine fragments are marked in the KEDs shown in Figure 10. While the low kinetic energy release into chlorine fragments from three-body decay does not allow a full kinematic analysis as outlined in section II, the qualitatively similar behavior of the fragments associated with three-body decay leads us to believe that this decay channel is accessed by a $\pi^*_{SO} \leftarrow n_S$ or $\pi^*_{SO} \leftarrow n_{Cl}$ excitation on the long wavelength edge of the second absorption band followed by a rapid redistribution of the excitation energy into the dissociation coordinate. Below the three-body limit, on the average Cl and Cl* atoms produced in channel (II) appear significantly slower (7250 and 6250 cm^{-1}, respectively) than the maximum value at 15800 cm^{-1}, which is given by the energetic threshold of 20040 cm^{-1} and indicated in Figure 10. This confirms an earlier observation where a new electronic state of SOCl at 9000 cm^{-1} has been postulated in order to explain this behavior.[43] On the other hand, significant vibrational fragment excitation was observed in the photodissociation of ozone[47] and OClO[48] and might also play an important role in the SOCl$_2$ decay, so the nature of SOCl excitation remains obscured. In any case, the pronounced anisotropic behavior of Cl and Cl* fragments associated with the radical channel (II) is evidence of a fast direct dissociation along the reaction coordinate, most probably following $\sigma^*_{SCl} \leftarrow n_S$ excitation on the short wavelength edge of the first absorption band. Secondary photolysis of SOCl is not of interest in this context and its minor participation in the

Feature Article

J. Phys. Chem. A, Vol. 104, No. 12, 2000 **2539**
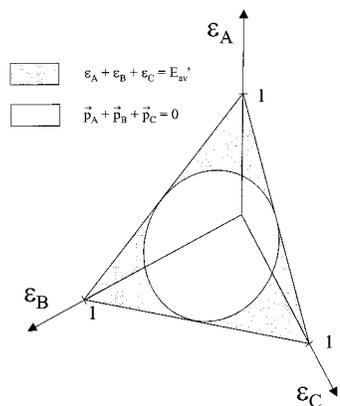
Figure 11. Energetically (gray) and kinematically (light gray) allowed areas in a three-dimensional Cartesian plot of fragment kinetic energies.

Figure 12. Dalitz plot representation derived from a proper projection of the triangularly shaped energetically allowed region of Figure 11. The elliptically shaped regions are kinematically allowed areas for $COCl_2$ and COFCl, respectively.

overall decay strongly depends on experimental conditions, i.e., mainly on laser fluence.

The observed data for $SO(X^3\Sigma^-)$ fragments fully confirm the conclusions drawn for the three-body decay. $SO(X^3\Sigma^-)$ generated in the photodissociation of $SOCl_2$ carries little kinetic and internal energy and only exhibits a weak spatial anisotropy. Hence, SO is a primary three-body decay product, and a contribution of a molecular decay channel into $SO(X^3\Sigma^-)$ + $Cl_2(v \gg 0)$, producing highly vibrationally excited chlorine molecules, is unlikely. While a production of electronically excited SO and ground state Cl_2 cannot be excluded, it does not affect the conclusions drawn on the above discussed mechanisms.

The overview given above demonstrates that a wealth of information is waiting to be gathered in this relatively unexplored field of reaction dynamics. This, at least in principle, favorable condition for the researcher brings up the question, however, on how to systematically define an appropriate language to descriptively characterize three-body decay processes. In the next and last section of this paper we wish to present one such language, namely, the use of so-called Dalitz plots.[49] The concept was originally developed to describe the three-body decay of a τ-meson into three identical π-mesons, and was later transferred to the investigation of chemical reactions involving equal fragment masses, like $A_3 + h\nu \rightarrow 3$ A.[8]

VII. Analysis Procedures

If internal energies E_i are neglected (or if the available energy is appropriately redefined as $E_{av}' = E_{av} - \sum E_i$), then the sum over the three fragment kinetic energies must be equal to the available energy, or if kinetic energies $\epsilon_i = T_i/E_{av}'$ are taken as percentages of the (redefined) available energy:

$$\sum \epsilon_i = 1 \qquad (8)$$

This condition imposes an energetic constraint on the fragment kinetic energy triples (ϵ_A, ϵ_B, ϵ_C) to lie on a triangularly shaped portion of a plane intersecting the kinetic energy axes of a Cartesian coordinate system at $\epsilon_i = 1$, as shown in Figure 11.

Additionally, there is a kinematic constraint based on the conservation of linear momentum:

$$\sum \vec{p}_i = \vec{0} \qquad (9)$$

which excludes, for example, the triples (1,0,0), (0,1,0), and (0,0,1). The kinematic constraint limits the value range to an elliptically shaped area on the energy triangle the exact shape
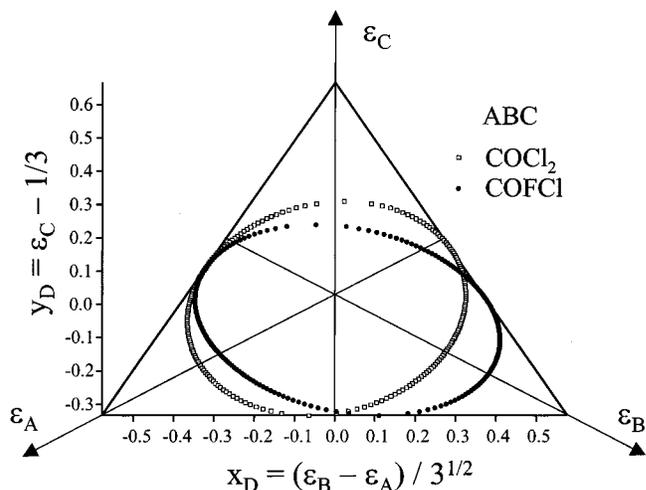
of which is given by the mass ratios of m_A, m_B, and m_C. The limiting ϵ_A and ϵ_B values for any given ϵ_C are determined from eq 7 if θ is set to 0 (forward scattering) and π (backward scattering).

If the axes of the coordinate system in Figure 11 are properly projected onto the triangular plane satisfying eq 8, then a Dalitz plot is obtained as shown in Figure 12. Here, the linear dependence of the three fragment kinetic energies has been employed in order to eliminate one of the three coordinates, and two new coordinates $x_D = (E_B - E_A)/\sqrt{3}$ and $y_D = E_C - {}^1/_3$ have been defined such that $(x_D, y_D) = (0,0)$ denotes equal partitioning of the fragment kinetic energies: $\epsilon_A = \epsilon_B = \epsilon_C = {}^1/_3$.[49] The original ϵ_i axes appear now as the three bisectrices of the equilateral triangle intersecting each other at an angle of 120°. Figure 12 shows the kinematically allowed areas beyond the case of identical fragments for the three-body decay of asymmetric molecules such as that of phosgene and of carbonyl chloride fluoride. The dynamics of the decay process determines which part of the allowed area inside the ellipses will be populated.

Every energetically and kinematically allowed energy triple ($\epsilon_A, \epsilon_B, \epsilon_C$) is represented by a point on or inside the ellipses in Figures 12 and 13. Consequently, the joint fragment KEDs translate into a density distribution of the respective allowed area. It should be noted that the Dalitz plot represents the joint probability distribution $P(E_i, T_i)$ for realizing a set of fragment energies E_i and T_i. Thus, in principle, it contains all available information on the decay dynamics. Here, the special merit of coincidence experiments is easily conceived in that they allow to experimentally determine every point of the Dalitz plot, whereas the Dalitz plot derived from experimentally observed single fragment KEDs from kinematic reasoning, as performed below, merely represents the simplest and most likely joint probability distribution in agreement with the chosen decay models.

It is easily conceived that a synchronous concerted decay, where $\epsilon_A = \epsilon_B$, is represented in the Dalitz plot by a vertical line at $x_D = 0$. Likewise, a sequential decay for a fixed energy deposition, and consequently for a fixed value of ϵ_C (and y_D), will be represented by a horizontal line, the exact position of which is determined by the energy deposition value E_{AB}. Forward scattering is to be found on the right hand side of the elliptic area (for $x_D > 0$), backward scattering on the left hand
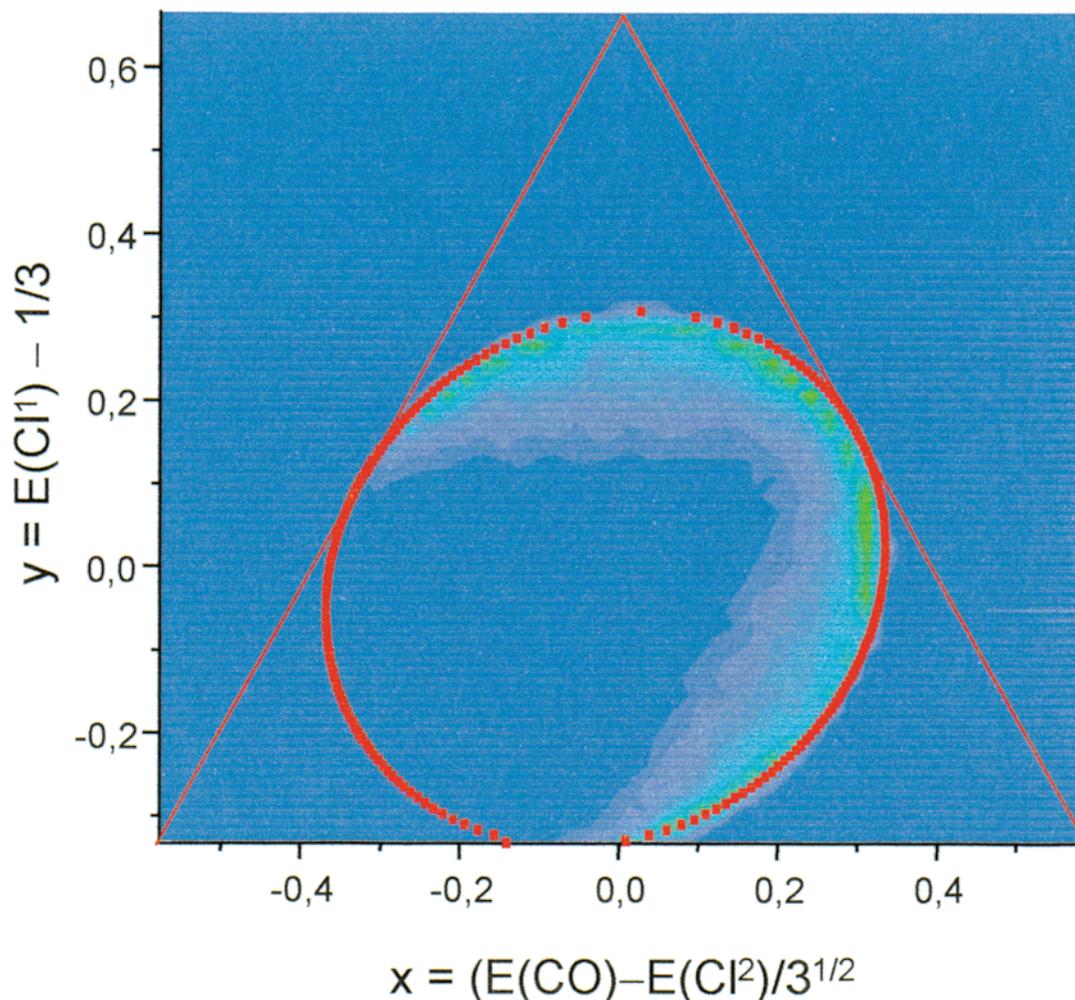
Figure 13. Density distribution in a Dalitz plot representation for the asynchronous concerted three-body decay of phosgene for the CO fragment quantum state $v = 1$, $J = 14$. Parameters: $\theta_0 = 180°$, $E_0(COCl) = 0.1E_{av}$.

side (for $x_D < 0$). Thus, any density distribution in the allowed area might be translated into a superposition of decay mechanisms, and vice versa. This will prove to be a highly versatile utility, if in coincidence measurements the density distribution in the Dalitz plot is directly measured, and the multitude of the obtained data awaits interpretation.

As a first application the asynchronous concerted decay of phosgene will be translated into Dalitz language by a Monte Carlo simulation, calculating how often a certain point in the Dalitz plot is realized, starting from the experimentally observed, known parameter distribution functions for the decay angle θ and for the energy deposition E_{AB} in the intermediate. Since the two Cl atoms are indistinguishable in the experiment, only ground state $Cl(^2P_{3/2})$ atoms are considered at the moment, the Dalitz plot density distribution must be symmetric with respect to the CO kinetic energy axis which runs from the upper right base to the lower left tip of the equilateral triangle in Figure 12, if the CO molecule is identified with fragment B. The parameter distributions obtained from the CO fragment KEDs are state specific distributions, as it is the case for the CO fragment KEDs themselves. As was discussed in the preceding section, the experimentally observed Cl atom KEDs, however, are a superposition of many different KEDs with CO partner fragments in a multitude of quantum states. Thus, from the quantum state specific parameter distribution the Monte Carlo simulation should reproduce the quantum state specific CO fragment KED, but not the experimentally observed, averaged

Cl atom KEDs. Also, of course only that part of the CO fragment KED will be reproduced which accounts for the simulated mechanism, here, the asynchronous concerted mechanism as the principal decay channel.

Figure 13 shows the result of 10^5 runs in a Monte Carlo simulation, where the input has been the parameter distributions obtained from the experimental data for the $CO(v = 1, J = 14)$ state. Approximately 80% of this state decays via the asynchronous concerted mechanism, characterized by Gaussian distributions of the decay angle α and the energy distribution E_{AB}, centered at $\alpha_0 = 182°$ with a width of 231° and at $E_{AB,0}$ 0.02 with a width of 0.1, which was extracted from former experiments.[6] The resulting Dalitz plot density distribution is characterized by the required symmetry with respect to the CO kinetic energy axis and by a pronounced enhancement of the density along the borders of the allowed area. The latter is a consequence of restricting the two-step decay mechanism to take place within the plane, originally defined by the parent phosgene molecule. No twisting is allowed in the course of the dissociation or, in other words, the fragment angular momentum vectors are confined to a perpendicular orientation with respect to the initial molecular plane. This assumption is justified by the fact that the atomic chlorine fragment cannot induce a nonperpendicular torque with respect to the parent molecule plane (if the small electronic angular momentum of the chlorine atom is neglected). Another approximation is done by neglecting the out-of-plane bending excitation of the parent molecule prior to the decay.

Feature Article

J. Phys. Chem. A, Vol. 104, No. 12, 2000 **2541**

If the Dalitz plot density distribution in Figure 13 is projected onto the CO fragment kinetic energy axis, the asynchronous concerted part of the CO fragment KED for $v = 1$, $J = 14$ is beautifully reproduced. Thus, it is proven that the interrelationship between the kinematic analysis and the Dalitz plot density distribution can be employed to illustratively interpret data from coincidence measurements in order to gain insight into the dynamics of the decay mechanisms.

VIII. Summary

The field of three-body reaction dynamics is an almost unknown terrain in today's physical chemistry, although three-body reactions participate in many complex reaction schemes in atmospheric and combustion chemistry. The photoinduced three-body decay can be studied by technologically advanced, challenging coincidence experiments as well as by established spectroscopic techniques if physically meaningful decay mechanisms and parameters are introduced. Such models have been presented, ranging from synchronous concerted via asynchronous concerted to purely sequential decay mechanisms.

A series of structurally similar molecules were investigated: phosgene, carbonyl chloride fluoride, and thionyl chloride. The phosgene studies yielded the most detailed results, in that the role of competing mechanisms could be determined and assigned to different exit channels via the X^1A_1 ground state and the A^1A_2 excited state potential energy surfaces. Carbonyl chloride fluoride behaves similar, but in a simpler way than the closely related phosgene, because the larger stability of the COF intermediate reduces the complexity brought about by decay channel competition and essentially served to confirm the phosgene results. Thionyl chloride has simultaneously been excited into two electronic excited states and therefore shows a competition between three- and two-body decay. Apart from that, the excitation into the second absorption band is comparable to the phosgene A^1A_2 state excitation and leads to comparable results.

New experimental techniques and novel analysis procedures promote the investigation of three-body decay processes. With the Dalitz plot representation a method was presented that is useful in bridging the gap between three-body decay studies performed by established methods and by novel coincidence methods and is expected to foster further research activity in this field.

IX. Acknowledgment

References and Notes

(1) Dömer, R.; Bräuning, H.; Feagin, J. M.; Mergel, V.; Jagutzki, O.; Spielberger, L.; Vogt, T.; Khemliche, H.; Prior, M. H., Schmidt-Böcking, H. *Phys Rev. A* **1998**, *57,* 1074.

(2) Dömer, R.; Bräuning, H.; Jagutzki, O.; Mergel, V.; Achler, M.; Moshammer, R.; Feagin, J. M.; Osipov, T.; Bräuning-Demian, A.; Schmidt-Böcking, H. *Phys Rev. Lett.* **1998**, *81,* 5776.

(3) Müller, U.; Eckert, T.; Braun, M.; Helm, H. *Phys. Rev. Lett.* **1999**, *83*, 2718.

(4) Norrish, R. G. W.; Crone, H. G.; Saltmarsh, O. D. *J. Chem. Soc.* **1934**, 1456.

(5) Kroger, P. M.; Riley, S. J. *J. Chem. Phys.* **1979**, *70,* 3863.

(6) Maul, C.; Gericke, K.-H. *Int. Rev. Phys. Chem.* **1997**, *16*, 1.

(7) Baer, T.; DePristo, A. E.; Hermans, J. J. *J. Chem. Phys.* **1982**, *76,* 5917.

(8) Strauss, C. E. M.; Houston, P. L. *J. Phys. Chem.* **1990**, *94,* 8751.

(9) Stranges, D.; Yang, X.; Chesko, J. D.; Suits, A.G. *J. Chem. Phys.* **1995**, *102,* 6067.

(10) Tanaka, Y.; Kawasaki, M.; Matsumi, Y.; Fujiwara, H.; Ishiwata, T.; Rogers, L. J.; Dixon, R. N.; Ashfold, M. N. R. *J. Chem. Phys.* **1998**, *109,* 1315.

(11) Lin, J. J.; Hwang, D. W.; Lee, Y. T.; Yang, X. *J. Chem. Phys.* **1998**, *108,* 10061.

(12) Mordaunt, D. H.; Ashfold, M. N. R.; Dixon, R. N. *J. Chem. Phys.* **1994**, *100,* 7360.

(13) Kim, S. K.; Pedersen, S.; Zewail, A. H. *J. Chem. Phys.* **95***, 103,* 477.

(14) Owrutsky, J. C.; Baronavski, A. P. *J. Chem. Phys.* **1998***, 108,* 6652.

(15) Zhong, Q.; Poth, L.; Castleman, A. W., Jr. *J. Chem. Phys.* **1999**, *110,* 192.

(16) Bañares, L.; Baumert, T.; Bergt, M.; Kiefer, B.; Gerber, G. *J. Chem. Phys.* **1998**, *108,* 5799.

(17) Gutmann, M.; Janello, J. M.; Dickebohm, M. S.; Grossekathöfer, M., Lindener-Roenneke, J. *J. Phys. Chem. A* **1998**, *102,* 4138.

(18) Jones, A. B.; Buxey, A. L. M.; Jukes, P. R.; Smith, J. A.; Stace, A. J. *J. Chem. Phys.* **1995**, *103,* 474.

(19) Jukes, P. R.; Buxey, A. L. M.; Jones, A. B.; Stace, A. J. *J. Chem. Phys.* **1999**, *109,* 5803.

(20) Hsieh, S.; Eland, J. H. D. *J. Phys. B: At. Mol. Opt. Phys.* **1997**, *30,* 4515.

(21) Hanold, K. A.; Luong, A. K.; Continetti, R. E. *J. Chem. Phys.* **1998**, *109,* 9215.

(22) Eland, J. H. D. *Meas. Sci. Technol.* **1994**, *5,* 1501.

(23) Jagutzki, O.; Mergel, V.; Ullmann-Pfleger, K.; Spielberger, L.; Meyer, U.; Dörner, R.; Schmidt-Böcking, H. In *Imaging Spectrometry IV*; Descour, M. R., Shen, S. S., Eds.; International Society for Optical Engineering: Bellingham, WA, 1998; Vol. 3438, p 32.

(24) Hsieh, S.; Eland, J. H. D. *J. Phys. B: At. Mol. Opt. Phys.* **1997**, *30,* 4515.

(25) Williams, M. B.; Sobottka, S. E. *IEEE Trans. Nucl. Sci.* **1989**, *36,* 227.

(26) Maul, C.; Haas, T.; Gericke, K.-H. J. *Phys. Chem. A* **1997**, *101,* 6619.

(27) Baum, G.; Effenhauser, C. S.; Felder, P.; Huber, J. R. *J. Phys. Chem.* **1992**, *96,* 756.

(28) Mordaunt, D. H.; Ashfold, M. N. R.; Dixon, R. *N. J. Chem. Phys.* **1994**, *100,* 7361.

(29) This definition for E_{AB} is equivalent with the definition of E_{av} with respect to the three-body decay into A, B, and C.

(30) Haas, T.; Maul, C.; Gericke, K.-H.; Comes, F. J. *Chem. Phys. Lett.* **1993**, *202,* 108.

(31) Braatz, C.; Tiemann, E. *Chem. Phys.* **1998**, *229,* 93.

(32) Arepalli, S.; Presser, N.; Robie, D.; Gordon, R. *Chem. Phys. Lett.* **1985**, *118,* 88.

(33) Loge, G. W.; Tiee, J. J.; Wampler, F. B. *J. Chem. Phys.* **1983**, *79,* 196.

(34) Okabe, H. *Photochemistry of Small Molecules*, Wiley, New York, 1978.

(35) Maul, C., Konkurrierende Dynamik beim Dreikörperzerfall von Molekülen, Wissenschafts-Verlag Dr. Maraun: Frankfurt, 1995.

(36) Haas, T.; Charakterisierung naszenter Photofragmente zur Aufklärung der Zerfallsdynamik von Stickstoffwas serstoffsäure und Phosgen, Wissenschafts-Verlag Dr. Maraun: Frankfurt, 1995.

(37) Moule, D. C.; Foo, P. D. *J. Chem. Phys.* **1971**, *55,* 1262.

(38) NIST−JANAF Thermochemical Tables. *J. Phys. Chem. Ref. Data* **1998** (Monograph 9).

(39) Herzberg, G. *Electronic Spectra of Polyatomic Molecules*; Van Nostrand Reinhold: New York, 1966.

(40) Uthman, A. P.; Demlein, P. J.; Aliston, T. D.; Withlam, M. C.; McClements, M. J.; Takacs, G. A. *J. Phys. Chem.* **1978**, *82,* 2252.

(41) Chen, X.; Asmar, F.; Wang, H.; Weiner, B. R. *J. Phys. Chem.* **1991**, *95,* 6415.

(42) Wang, H.; Chen, X.; Weiner, B. R. *J. Phys. Chem.* **1993**, *97,* 12260.

(43) Baum, G.; Effenhauser, C. S.; Felder, P.; Huber, J. R. *J. Phys. Chem.* **1992**, *96,* 756.

(44) Baum, G. Zur Photodissoziation eines Moleküls mit zwei äquivalenten Bindungen. Ph.D. Thesis, Universität Zürich, 1993.

(45) Kawasaki, M.; Kasatani, K.; Sato, H.; Shinohara, H.; Nishi, N.; Ohtoshi, H.; Tanaka, I. *Chem. Phys.* **1984**, *91,* 285.

(46) Maul, C.; Roth, M.; Gericke, K.-H. To be published.

(47) Miller, R. L.; Suits, A. G.; Houston, P. L.; Toumi, R.; Mack, J. A.; Wodtke, A. M. *Science* **1994**, *263,* 1831.

(48) Roth, M.; Maul, C.; Gericke, K.-H. *J. Chem. Phys.* **1997**, *107,* 10582.

(49) Dalitz, H. R. *Philos. Mag.* **1953**, *44,* 1068.